Structural Engineering and Mechanics, Vol. 14, No. 2 (2002) 119-133
DOI: http://dx.doi.org/10.12989/sem.2002.14.2.119

The fiber element technique for analysis of concrete-filled steel tubes under cyclic loads

A.A. Golafshani†

Department of Civil Engineering, Sharif University of Technology, Tehran, Iran

S.B.B. Aval‡

Department of Civil Engineering, North Carolina State University, Raleigh, NC 27695, USA

M.A. Saadeghvaziri‡†

Department of Civil and Environmental Engineering, NJIT, Newark, NJ-USA

(Received October 2, 2000, Accepted May 9, 2002)

Abstract. A beam-column fiber element for the large displacement, nonlinear inelastic analysis of Concrete-Filled Steel Tubes (CFT) is implemented. The method of description is Total Lagrangian formulation. An 8 degree of freedom (DOF) element with three nodes, which has 3 DOF per end node and 2 DOF on the middle node, has been chosen. The quadratic Lagrangian shape functions for axial deformation and the quartic Hermitian shape function for the transverse deformation are used. It is assumed that the perfect bond is maintained between steel shell and concrete core. The constitutive models employed for concrete and steel are based on the results of a recent study and include the confinement and biaxial effects. The model is implemented to analyze several CFT columns under constant and non-proportional fluctuating concentric axial load and cyclic lateral load. Good agreement has been found between experimental results and theoretical analysis.

Key words: Concrete-Filled steel Tubes (CFT); composite fiber element; cyclic loads; hysteretic; material models; Lagragian shape functions; Hermitian shape functions; quartic shape functions.

1. Introduction

It is widely recognized that the innovative use of two or more material in structures generally leads to more efficient economical systems for resisting seismic forces. In this area utilizing of Concrete-Filled steel Tubes (CFT) are new idea which increasingly finding application in design practice. In spite of excellent advantages, designers rarely utilize CFT systems, since few practical nonlinear frame models have been developed to simulate the important aspects of CFTs. Some

† Assistant Professor
‡ Postdoctoral Fellow
‡† Professor

advantages of them are:

1. During construction the steel shell acts as both erection steel and forming for composite column, decreasing the labor and material required for construction and, consequently, lowering the construction cost.
2. The steel shells not only improve axial strength but also increases flexural and shear resistance of column as its location at the perimeter. Therefore it acts as longitudinal and transverse reinforcement.
3. Interaction between the steel shell and the concrete core causes that the concrete core prevents inner directional buckling of steel shell, thus shifts its mode into higher mode. Otherwise, the steel shell provides confinement for concrete core thus causes the ductility and strength of core increases.
4. The experiments show good seismic characteristics and energy absorption.
5. CFTs have lighter cross section in comparison to ordinary reinforced concrete column under specific loads and height.
6. They experience smaller deformation than RC due to higher geometric sectional characteristics.
7. They show lower creep and shrinkage effects.

The use of CFTs in structural frames has increased in United States, Japan, China and Australia during the past ten years. They have been used as columns or bracings, piers for bridges, and columns for high-rise buildings.

2. Previous research

For an in-depth review of analytical and experimental research on CFT columns the reader is referred to Shams and Saadeghvaziri (1997). In general, there have been many experimental studies of CFT columns; however the literatures are scarce with regard to analytical works. Now few computational researches conducted on cyclic load-deformation of CFTs and much of the works focused on computing the ultimate axial and flexural capacity of members (e.g., Kloppel and Goder 1957, Knowles and Park 1969 &1970, Neogi and San 1969, Kato and Shohara 1978, Wakabayashi and Minami 1981).

Ge and Usami (1994), and Shams (1999) used nonlinear three dimensional analyses into rectangular and circular CFT stub box columns. To reduce the computational effect, researchers have proposed the “line” element approaches. Hajjar and Gourley (1996, 1997) and Hajjar *et al*. (1998a, 1998b) have applied this type of element to study of the nonlinear response of CFTs. The original studies consist of development of a concentrated plasticity finite element model for CFT members. The more recent work is a fiber-based distributed plasticity finite element formulation, which is less compact than the concentrated plasticity model. The authors (Aval *et al*. 2002) have also performed one of the most recent and through analytical works on the performance of CFT columns. It consists of two beam components for the concrete core and steel shell. The bond/slip formulation represents slippage between steel shell and concrete core. However these methods include additional degree of freedom at the element ends, allowing the concrete and the steel to have independent displacements and rotations. When modeling the frames using CFT, it is difficult to enforce the compatibility conditions at the semi-rigid composite connection. Furthermore, in the aforementioned study, it was concluded that the effect of bonding on ultimate strength is less pronounced.

In this research work, an inelastic fiber element is proposed to provide the necessary degree of accuracy for studying of CFT columns. This element is so useful to do practical analysis of frame structures with CFT columns with less degree of freedom.

3. Solution strategy

The scope of this research is to develop an element to demonstrate nonlinear behavior of CFTs under cyclic as well as monotonic loads. This one-dimensional element works in plane. Extension to the 3-D case is straightforward.

In driving of formulation following assumptions are proposed:

1. Plane sections of the concrete core and the steel shell before and after bending remain plane.
2. Shear deformations due to the size of the section are negligible.
3. During loading history the shell will not buckle. This assumption has a negligible effect on results for moderate and low aspect ratio that usually used in practice.
4. Effects of confinement on concrete and biaxial state of stress in the steel shell are accounted for through the uniaxial material models using recent results (Shams and Saadeghvaziri 1999).
5. The effects of creep and shrinkage are neglected because they have a small influence on the behavior of CFTs (Nakai *et al.* 1991); and
6. Effects of residual stresses are neglected.

4. Element description

The proposed element has three nodes and it has 3 DOFs on each ends and 2 DOF on middle node with total of 8 DOFs (Fig. 1).

Based on the definition of Green strain for geometrically nonlinear behavior and the assumption of planar sections remains plane during deformation, the generalize strain can be expressed as follow:

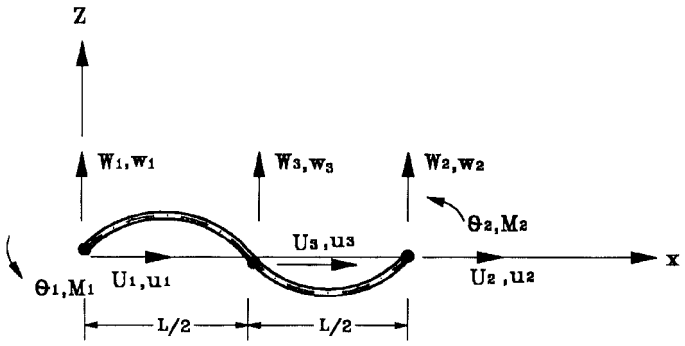

Fig. 1 Element's degree of freedom

$$\boldsymbol{d} = \begin{Bmatrix} \bar{\varepsilon} \\ \chi \end{Bmatrix} = \begin{Bmatrix} u'(x) + \frac{1}{2}w'^2(x) \\ -w''(x) \end{Bmatrix} \tag{1}$$

This can be separated into linear and nonlinear parts as:

$$\boldsymbol{d} = \boldsymbol{d}_1 + \boldsymbol{d}_n;\ \boldsymbol{d}_1 = \begin{Bmatrix} u'(x) \\ -w''(x) \end{Bmatrix};\ \boldsymbol{d}_n = \begin{Bmatrix} \frac{1}{2}w'^2(x) \\ 0 \end{Bmatrix} \tag{2}$$

The displacement fields are $u(x)$ and $w(x)$ which are the axial and transversal displacement of reference axis of beam respectively.

The corresponding generalized stresses are:

$$\boldsymbol{D} = \begin{Bmatrix} N(x) \\ M(x) \end{Bmatrix} \tag{3}$$

$N(x)$ and $M(x)$ are the sectional axial force and the sectional bending moment respectively.

The nodal degree of freedom and corresponding nodal forces:

$$\boldsymbol{q}^T = (\boldsymbol{q}_u, \boldsymbol{q}_w)\ ;\ \boldsymbol{Q}^T = (\boldsymbol{Q}_u, \boldsymbol{Q}_w) \tag{4}$$

Where

$$\boldsymbol{q}_u^T = (u_1, u_2, u_3)\ ;\ \boldsymbol{q}_w^T = (w_1, \theta_1, w_2, \theta_2, w_3) \tag{5a}$$

$$\boldsymbol{Q}_u^T = (U_1, U_2, U_3)\ ;\ \boldsymbol{Q}_w^T = (W_1, M_1, W_2, M_2, W_3) \tag{5b}$$

The quadratic Lagrangian shape functions for axial deformation and the cubic quartic Hermitian shape function for transverse direction are used. The explicit forms of these functions are:

$$\boldsymbol{N}_u^T = (1 - 3\xi + 2\xi^2, -\xi + 2\xi^2, 4\xi - 4\xi^2) \tag{6a}$$

$$\begin{aligned} \boldsymbol{N}_w^T = {} & (1 - 11\xi^2 + 18\xi^3 - 8\xi^4, (\xi - 4\xi^2 + 5\xi^3 - 2\xi^4)L, \\ & -5\xi^2 + 14\xi^3 - 8\xi^4, (\xi^2 - 3\xi^3 + 2\xi^4)L, 16\xi^2 - 32\xi^3 + 16\xi^4) \end{aligned} \tag{6b}$$

Where ξ is non-dimensional co-ordinate and described as $\xi = x/L$

The virtual displacement work equation can be expressed as:

$$\delta V = \int \boldsymbol{D}^T \cdot \delta \boldsymbol{d}\ dx - \boldsymbol{Q}_e^T \delta \boldsymbol{q} \tag{7}$$

$\boldsymbol{Q}_e$ = External nodal force vector

The linear and nonlinear generalized strains based on differentiation of displacement field are:

$$\boldsymbol{d}_1 = \boldsymbol{B}_1\boldsymbol{q} \;\; ; \;\; \boldsymbol{d}_n = \frac{1}{2}\boldsymbol{B}_n\,\boldsymbol{q} \tag{8}$$

Where:

$$\boldsymbol{B}_1 = \begin{bmatrix} \boldsymbol{B}_u & \boldsymbol{0} \\ \boldsymbol{0} & \boldsymbol{B}_\chi \end{bmatrix} \;\; ; \;\; \boldsymbol{B}_n = \begin{bmatrix} \boldsymbol{0} & \boldsymbol{q}_w^T\boldsymbol{A}_w \\ \boldsymbol{0} & \boldsymbol{0} \end{bmatrix} \tag{9}$$

In which:

$$\frac{du(x)}{dx} = \boldsymbol{B}_u\boldsymbol{q}_u \;\; ; \;\; \frac{dw(x)}{dx} = \boldsymbol{B}_w\boldsymbol{q}_w \;\; ; \;\; -\frac{d^2w(x)}{dx^2} = \boldsymbol{B}_\chi\boldsymbol{q}_w \tag{10}$$

And:

$$w'^2 = \boldsymbol{q}_w^T\boldsymbol{A}_w\boldsymbol{q}_w \;\; ; \;\; \boldsymbol{A}_w = \boldsymbol{B}_w^T\boldsymbol{B}_w \tag{11}$$

So $\boldsymbol{A}_w$ is a symmetric matrix.

With substitution of generalized strain in expression of (7), it can be expressed as:

$$\delta V = [\int \boldsymbol{D}^T \cdot \delta(\boldsymbol{d}_1 + \boldsymbol{d}_n)dx] - \boldsymbol{Q}_e^T\delta\boldsymbol{q} \tag{12}$$

$$\delta V = [\int \boldsymbol{D}^T \cdot (\boldsymbol{B}_n + \boldsymbol{B}_1)dx]\,\delta\boldsymbol{q} - \boldsymbol{Q}_e^T\delta\boldsymbol{q} = \boldsymbol{Q}_i^T\delta\boldsymbol{q} - \boldsymbol{Q}_e^T\delta\boldsymbol{q} = 0 \tag{13}$$

Therefore the internal nodal force vector is:

$$\boldsymbol{Q}_i = \int(\boldsymbol{B}_n + \boldsymbol{B}_1)^T\boldsymbol{D}dx = \int\boldsymbol{B}_{nl}^T\boldsymbol{D}dx \tag{14}$$

The tangent stiffness matrix obtains from differentiation of the internal nodal force vector with respect to the nodal displacement vector:

$$\boldsymbol{K}_t = \frac{\partial\boldsymbol{Q}_i}{\partial\boldsymbol{q}} = \int\frac{\partial(\boldsymbol{B}_{nl}^T\boldsymbol{D})}{\partial\boldsymbol{q}}dx = \int\frac{\partial(\boldsymbol{B}_n^T\boldsymbol{D})}{\partial\boldsymbol{q}}dx + \int\boldsymbol{B}_1^T\frac{\partial\boldsymbol{D}}{\partial\boldsymbol{q}}dx \tag{15}$$

By substituting:

$$\frac{\partial\boldsymbol{D}}{\partial\boldsymbol{q}} = \frac{\partial\boldsymbol{D}}{\partial\boldsymbol{d}}\frac{\partial\boldsymbol{d}}{\partial\boldsymbol{q}} = \boldsymbol{k}_s\boldsymbol{B}_{nl} \;\; ; \;\; \frac{\partial\boldsymbol{D}}{\partial\boldsymbol{d}} = \boldsymbol{k}_s \;\; ; \;\; \frac{\partial\boldsymbol{d}}{\partial\boldsymbol{q}} = \boldsymbol{B}_{nl} \tag{16}$$

in Eq. (15), yield the tangent stiffness matrix in the following simple form:

$$\boldsymbol{K}_t = \int[N(x)\boldsymbol{C} + \boldsymbol{B}_{nl}^T\boldsymbol{k}_s\boldsymbol{B}_{nl}]dx \;\; ; \;\; \boldsymbol{C} = \begin{bmatrix} \boldsymbol{0} & \boldsymbol{0} \\ \boldsymbol{0}^T & \boldsymbol{A}_w \end{bmatrix}_{8\times 8} \tag{17}$$

$\boldsymbol{k}_s$ is the tangent section stiffness matrix that depends on nonlinear loading history property of material section and it is defined as a 2×2 matrix.

$$\boldsymbol{k}_s = \begin{bmatrix} EA & EX \\ EX & EI \end{bmatrix} \tag{18}$$

Where *EA*, *EX*, and *EI* are axial, cross-coupling and flexural stiffness of section respectively which depend on nonlinear history of material section. In the beginning of loading the material is elastic and so *EX* is zero, but after entrance to nonlinearly range this product will became nonzero. The quadratic Lagragian shape functions are used for axial deformation. In order to ameliorate the membrane locking the reduced order of integration is used.

For frame with prismatic members in linear elastic domain the use of Hermitian polynomials for flexural deformation in transverse direction causes exact solution, which means a linear curvature distribution within the member. This assumption deviates significantly from the actual curvature distribution, for highly nonlinear element behavior, which causes serious numerical difficulties. For the sake of accuracy, more elements must be used in each member. The use of quartic Hermitian shape functions can improve the conditioning of the tangent stiffness matrix. The other benefit of using higher order shape function is one can imply the more number of sample points in numerical integration that can represent the spread of inelastic stresses in CFTs. Adequate accuracy is reached using Gauss-Lobatto integration method. This integration method allows for two integration points to coincide with the end sections of the element, where significant inelastic deformations typically take place.

5. Fiber element technique

One of the most promising methods for accurate modeling of the nonlinear analysis of reinforced concrete beam and column sections is the fiber element approach.

The values of *EA*, *EX*, and *EI* in Eq. (18) at integration points must be evaluated during deformation history. For this purpose the sections at integration's points are divided into small areas where the size of them depended on desired accuracy (Fig. 2). The load history for each fiber according to uniaxial stress-strain relationship should be recorded. This process is complete by summation for each fiber i.e.,

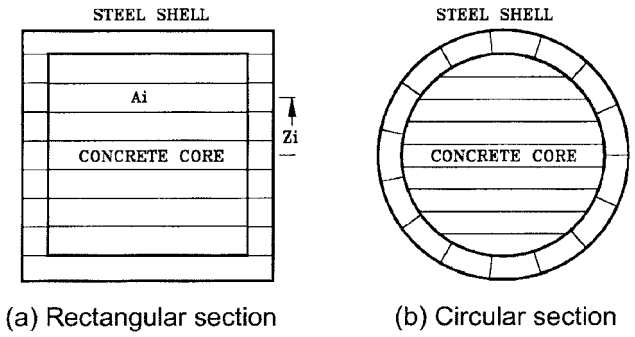

Fig. 2 Dividing of CFT cross section to fibers

$$EA = \sum_{i=1}^{nfiber} E_i^T \cdot A_i \;\; ; \;\; EX = \sum_{i=1}^{nfiber} E_i^T \cdot A_i Z_i \;\; ; \;\; EI = \sum_{i=1}^{nfiber} E_i^T \cdot A_i \cdot Z_i^2 \tag{19}$$

The cyclic uniaxial behaviors of the constituent materials (namely, steel and concrete) are illustrated in the next section.

6. Material behavior

The fiber element formulation simplifies the task of material model selection to uniaxial behavior, which is well established to date. Three-dimensional effects on the material behavior can be included into the uniaxial model by appropriate modification of parameters that define the monotonic envelope curve.

7. Concrete model

In order to compute the stress in each point due to calculated strain, a material law describing the concrete stress-strain relation under arbitrary cyclic strain histories is needed. The model employed in this study is the one proposed by Mohd Yassin (1994). The monotonic envelope curve of concrete in compression follows the model of Kent and Park (1971) as extended by Scott *et al.* (1982). The concrete damage considered in this model is in the form of unloading and reloading stiffness degradation for increasing values of the maximum strain. The reduction of the monotonic envelope under cyclic loading is not taken into account in this model. The tensile behavior of the model takes into account tension stiffening and the degradation of the unloading and reloading stiffness for increasing values of the maximum tensile strain after initial cracking. A linear rate of tensile strength reduction is adopted in this model.

It is well known that for concrete confinement has a significant effect on its maximum compressive strength and strain at the maximum stress. However, due to the nature of confinement stress distribution, this effect is not similar for rectangular and circular cross sections (Shams and Saadeghvaziri 1999). Furthermore, for CFT columns other geometric factors such as aspect ratio significantly affect the degree of confinement. Aspect ratio is defined as the ratio of the cross section diameter (or width) to the thickness of the steel shell. In this study the equations recently proposed by Shams and Saadeghvaziri (1999) for the maximum confined strength and corresponding strain are employed. For example, the expression for the maximum confined stress, f'_{cc}, has the following form:

$$f'_{cc} = f'_c \left(1 + \frac{A}{1 + \left(\frac{D/t}{B} \right)^{\alpha}} \right) \tag{20}$$

Where, f'_c is the uniaxial compressive strength, D/t is the aspect ratio, α is shape factor, and A and B are empirical parameters expressed in terms of f'_c.

8. Steel model

The nonlinear model of Menegotto and Pinto (1973), as modified by Filippou *et al*. (1983) to also include isotropic strain hardening describes the steel shell stress-strain behavior. In this model elastic and yield asymptotes are assumed to be straight lines, the position of the limiting asymptotes corresponding to the yield surface is assumed to be fixed at all times and the unloading slope remains constant and equal to initial slope.

The maximum stresses that steel tube in CFT columns can sustain depends mainly on the aspect ratio (D/t) and length-width ratio (L/D). Steel tube under biaxial state of stress exhibits a lower yield stress. In the case of short columns, the level of decrease in the yield stress depends on the aspect ratio and cross-sectional shape (Shams and Saadeghvaziri 1999). Similar to the concrete material, the expression given by Shams and Saadeghvaziri (1999) is used to consider the biaxial effect for the steel tube.

9. Verification studies

The proposed beam element is implemented in the nonlinear finite element program FEAP developed by Professor Taylor (1998) at the University of California, Berkeley. For demonstrating the versatility of the fiber element some examples are illustrated as follow.

10. Sakino CFT beam-columns

This example verifies the monotonic and cyclic behavior of proposed CFT fiber element in comparison with experimental results. Table 1 shows the mechanical properties of the two rectangular sections, which are experimented by Sakino and Tomii (1981), and Sakino and Ishibashi (1985). Fig. 3 represents the overall view of CFT beam-column experiments. The type of test is non-proportional loading. After completion of applying the axial load, the monotonic or the cyclic lateral displacements were applied. For simplicity and comparison of results only one cycle of displacements in each displacement level is applied as shown in Fig. 4.

Five Gauss Lobatto integration points with three elements in member are utilized. Fig. 5 illustrates

Table 1 Specifications of concrete-filled steel tubes

Test	Type of Test	N (kN)	N/N_0	Tube Dimensions (mm)	L/D	D/t	f_c' (Mpa)	$Z^{\dagger}$	f_y (Mpa)
SI85-I♣	M*	140	0.19	SQ 100 × 100 × 4.25	3.0	24	22.5	1.83	322
SI85-II	M*	89	0.18	SQ 100 × 100 × 2.20	3.0	45	20.9	4.08	297
ST81-I♣♣	C**	124	0.20	SQ 100 × 100 × 4.21	6.0	24	20.4	2.01	296
ST81-II	C**	108	0.20	SQ 100 × 100 × 2.96	6.0	34	22.9	2.95	299

M*= Monotonic ; C**= Cyclic

†Descending slope of stress-strain curve of concrete.

♣Sakino and Ishibashi (1985). ♣♣Sakino and Tomii (1981).

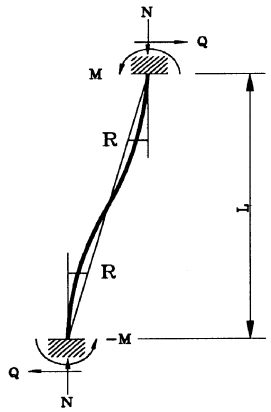

Fig. 3 Overall view of CFT beam-column experiments

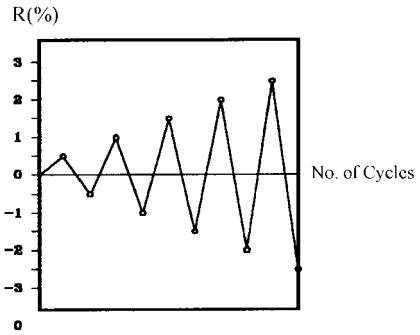

Fig. 4 Loading history

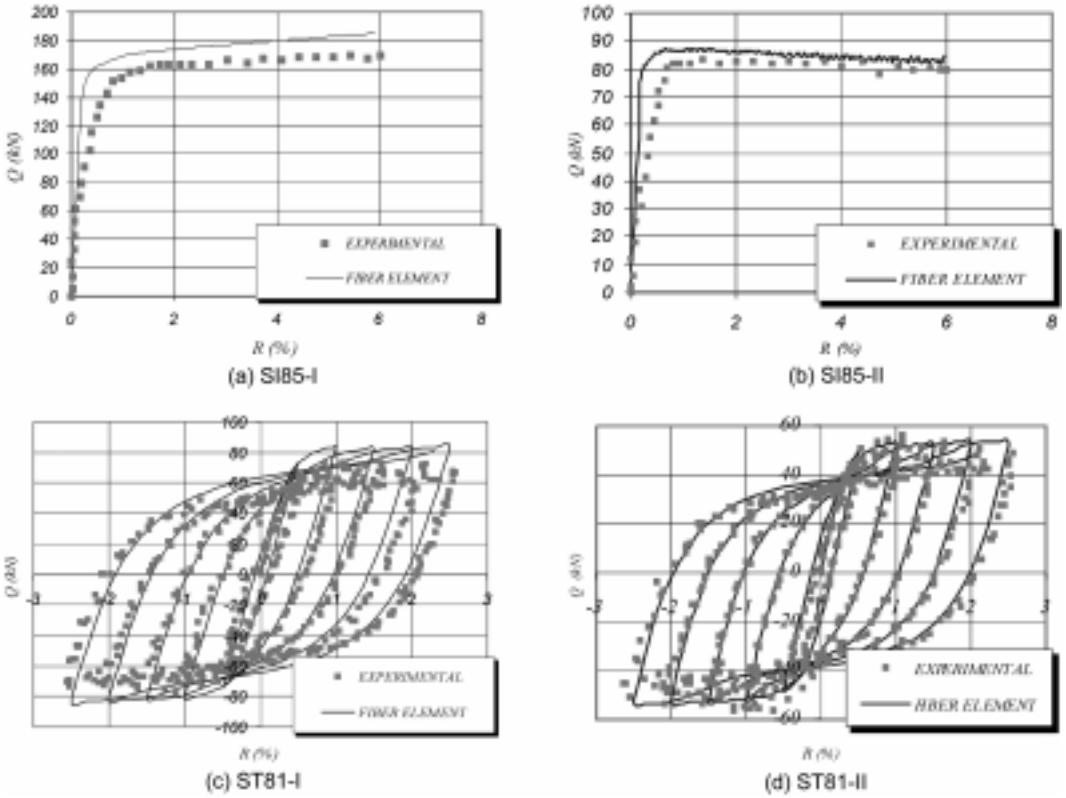

Fig. 5 Lateral load-displacement curves (experimental and analytical) for monotonic displacements as well as cyclic displacements

the correlation results from fiber element model versus the experimental results that are performed by Sakino and Ishibashi for monotonic loading and Sakino and Tomii for cyclic loading

respectively. It is observed, there is a good agreement between analytical results and the experiments not only for monotonic loads but also for cyclic loads.

Some deviation near the yield plateau is observed. The analytical results show higher strength in comparison with the experimental results. These are due to local buckling of the steel shell, which are not considered in the analytical model. From Fig. 5a, b could be concluded that the larger the *D*/*t* ratio, the more prominent the decrease in shear resistance through inelastic range. This is due to more predominant of the softening behavior of concrete part respect to stiffening behavior of steel part in analytical approach.

According to Fig. 5c, d the proposed elements evaluate accurately the hysteretic characteristic of CFT column. In last cycles, the experimental results show higher strength degradation with respect to analytical results. Again, this is mainly due to local buckling and fracture of the steel shell at high level of lateral displacement.

11. CFT column under non-proportionally fluctuating axial Load

For demonstrating the versatility of proposed element to support the complex loads, non-proportionally fluctuating axial load and simultaneously controlled cyclic lateral displacements are applied on top of the ST81 column in previous example. The loading and displacement patterns are illustrated in Fig. 6 and resulted hysteretic loops are shown in Fig. 7a. For comparison of behavior of CFT columns with a RC columns under such complex loading, one loop of hysteretic curve for RC column under the same loading pattern that was recognized by Saadeghvaziri and Foutch (1990) is represent in Fig. 7b.

Note when structures are under the combined effects of vertical and horizontal earthquake motion, the columns stand the uncouple variation in axial and lateral loads. Even though the hysteretic loops show a pinching and thin shape, but contrast to RC column, the hysteretic curve of this CFT column is of the Masing type (Saadeghvaziri and Foutch 1990). This behavior is mainly from ductile behavior of concrete core, which is due to proper confinement of encased concrete in CFT columns respect to RC columns that the concrete is confined with ties or spirals. This phenomenon causes dissipation of earthquake excitation. This example shows a superior behavior of CFT than RC to response complex earthquake motions.

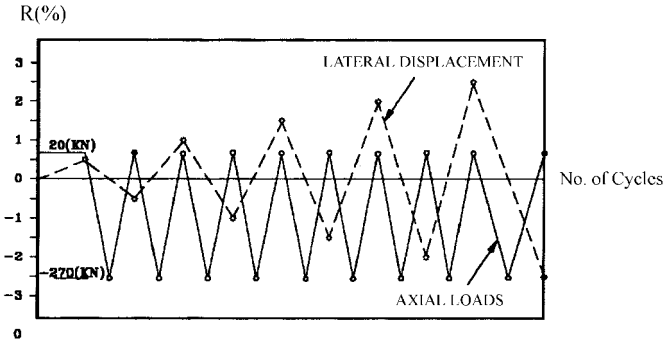

Fig. 6 Displacement and loading patterns for non-proportionally loading

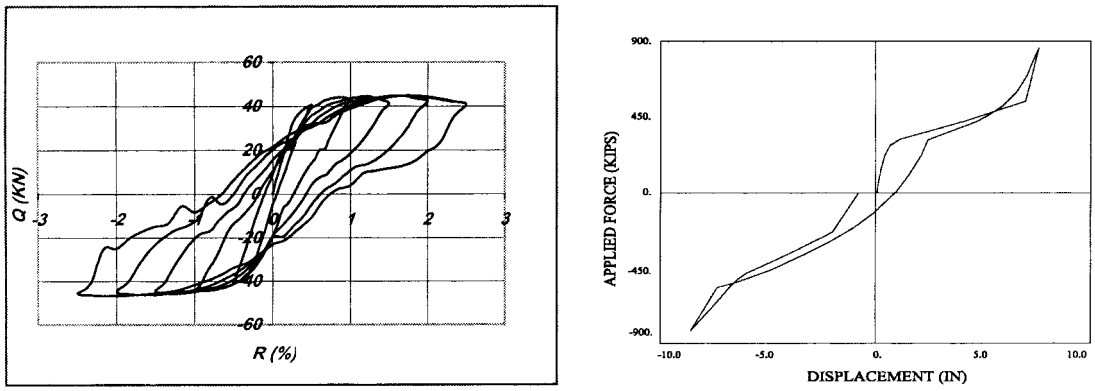

(a) CFT column (b) Typical RC columns

Fig. 7 Lateral force-deformation hysteretic loops under non-proportional axial load

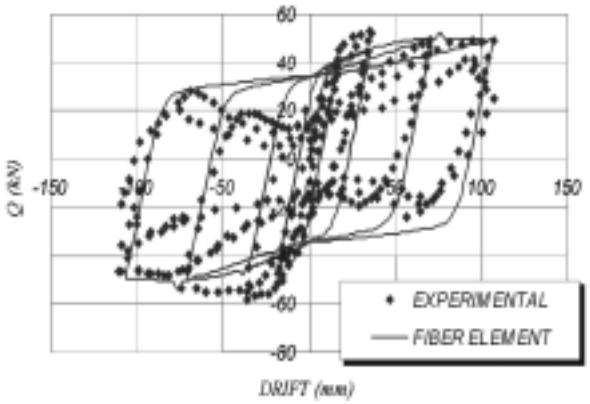

Fig. 8 Lateral load-displacement curves (experimental and analytical) for circular CFT column with high aspect ratio under cyclic loads

12. Boyd and Sugano beam-column

In this example a cantilever circular CFT column with 203 millimeter (8 in) diameter and 3 millimeter (0.109 in) thick shell is acted under history loads. The yield strength of the steel shell is 345 Mpa and the cylindrical strength of concrete core is 32 Mpa. The axial load was maintained at a constant level of 178 kN ($N/N_0 = 0.15$). This is the sample No.1 of the experiments that was done by Boyd *et al*. (1995).

The loading sequence was similar to the procedures used by Priestley and Park (1987). Analysis was subjected to a simulated seismic loading pattern consisting of increasing multiples of lateral displacement at free end to demonstrate the ductility and hystertic behavior of the test specimen.

The pinching which is observed in experiments is due to high potential for buckling due to high width to thickness ratio ($D/t = 73$). The analytical model can estimate the maximum strength of column in each cycle well, but it is less accurate for tracing the loading history for CFT column

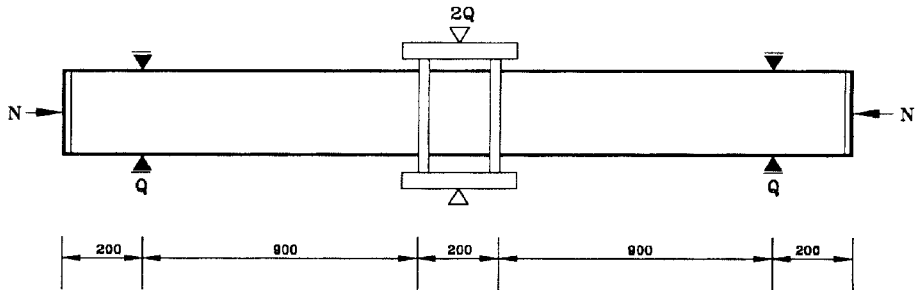

Fig. 9 Typical test (Sugano and Nagashima 1992)

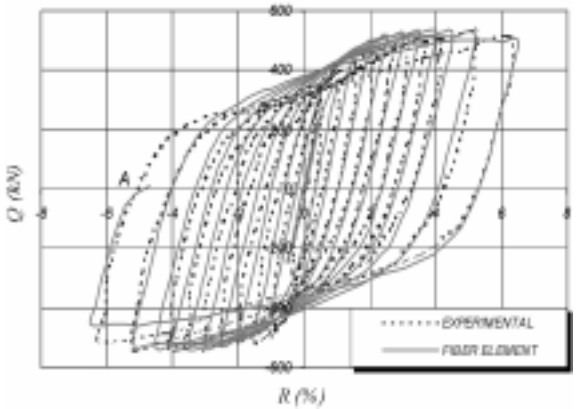

Fig. 10 Lateral load-displacement curves (experimental and analytical) for circular CFT column with low aspect ratio under cyclic loads

with a high aspect ratio (Fig. 8).

The similar experiment was done by Sugano and Nagashima (1992). The Fig. 9 shows the illustration of specimen and loading. This CFT column has a circular section with 300-millimeter diameter and 8 millimeter thick shell. The yield strength of the steel shell is 400 Mpa and the cylindrical strength of concrete core is 37 Mpa. The level of axial force is $N/N_0 = 0.3$. The aspect ratio of this column is 37, which approximately is the half of the previous experiments. The hysteretic loops are shown in Fig. 10. We observe, the shape is stable and the proposed element can precisely evaluate the cyclic behavior of the column. At point 'A' on analytical curve, the solution didn't converge. It was due to sever cracking and crushing of concrete.

Therefore the element has good accuracy for modeling of CFT columns with aspect ratio less than about 40.

13. Conclusions

An inelastic fiber element is developed for practical analysis of composite systems such as CFT columns. The proposed composite inelastic fiber element proves to be very reliable under monotonic

as well as cyclic loading, and it traces the experimental results with good accuracy. The versatility is due to the fact that no predefined phenomenological rules are involved in dictating the overall hysteretic behavior of any cross section. Under the assumption of uniaxial state of stress, only the stress-strain properties of the constituent material are required to define the properties of any cross section. Furthermore, using the results of a recent study (Shams and Saadeghvaziri 1999) the confinement and biaxial effect are considered. When the local buckling potential is low i.e., a CFT column with low to moderate aspect ratio (under 40) the element can trace deformation history under any arbitrarily loading.

Acknowledgements

This research was conducted as part of Dr. S.B.B. Aval PhD dissertation. United Nations' TOKTEN Program provided the opportunity for the third author for his participation in this study. The writers would like to thank to Prof. Taylor of the University of California, Berkeley for his efforts to enhance program FEAP.

References

Aval, S.B.B., Saadeghvaziri, M.A. and Golaafshani, A.A. (2002), "A comprehensive composite inelastic fiber element for cyclic analysis of CFT columns", *J. Eng. Mech*., ASCE, **128**(4).

Boyd, P.F., Cofer, W.F. and Mclean, D.I. (1995), "Seismic performance of steel encased concrete columns under flexural loading", *ACI Struct. J.*, **92**(3), 355-364.

Filippou, F.C., Popov, E.P. and Bertero, V.V. (1983), "Effects of bond deterioration on hysteretic behavior of reinforced concrete joints", *EERC Report 83/19, Earthquake Engineering Research Center*, University of California, Berkeley.

Ge, H.B. and Usami, T. (1994), "Strength analysis of concrete-filled thin-walled steel box column", *J. Constr. Steel Res*., **30**(3), 259-281.

Hajjar, J.F. and Gourley, B.C. (1996), "Representation of concrete-filled steel tube cross-section strength", *J. Struct. Eng.*, **122**(11).

Hajjar, J.F. and Gourley, B.C. (1997), "A cyclic nonlinear model for concrete-filled tubes", *J. Struct. Eng.*, **123**(6).

Hajjar, J.F., Schiller, P.H. and Molodan, A. (1998a), "A distributed plasticity model for concrete-filled steel tube beam-columns and composite frames", *Eng. Struct*., **20**(4-6), 398-412.

Hajjar, J.F., Molodan, A. and Schiller, P.H. (1998b), "A distributed plasticity model for cyclic analysis of concrete-filled steel tube beam-columns with interlayer slip", *Eng. Struct*., **20**(8), 663-676.

Kato, B. and Shohara, R. (1978), "Strength of steel-reinforced concrete members", *Transactions of the Architectural Institute of Japan*, No. 266. (in Japanese).

Kent, D.C. and Park, R. (1971), "Flexural members with confined concrete", *J. Struct. Div.*, ASCE, **97**(7).

Kloppel, V.K. and Goder, W. (1957), "An investigation of the load carrying capacity of concrete-filled steel tubes and development of design formula", *Der Stahlbau*, **26**(1).

Knowels, R. and Park, R. (1969), "Strength of concrete filled steel tubular columns", *J. Struct. Div.*, ASCE, **95**(12).

Knowels, R. and Park, R. (1970), "Axial load design for concrete filled steel tubes", *J. Struct. Div.*, ASCE, **96**(10).

Menegotto, M. and Pinto, P.E. (1973), "Method of analysis for cyclically loaded reinforced concrete plane frames including changes in geometry and non-elastic behavior of elements under combined normal force and bending", *Proceedings, IABSE Symposium on Resistance and Ultimate Deformability of Structures Acted on*

by Well Defined Repeated Loads", Lisbon, 15-2.
Mohd Yassin, M.Y. (1994), "Nonlinear analysis of prestressed concrete structures under monotonic and cyclic loads", Ph.D. Dissertation, Department of Civil Engineering, University of California, Berkeley.
Nakai, H., Kurita, and Ichinose, L.H. (1991), "An experimental study on creep of concrete filled steel pipes", *Proc., 3rd Int. Conf. Steel-Concrete Compos. Struct.*, M. Wakabayashi, ed., Assn. For Int. Cooperation and Res. In steel-Concrete Compos. Struct., 55-65.
Neogi, P.K. and San, H.K. (1969), "Concrete filled tubular steel columns under eccentric loading", *J. Struct. Eng.*, **47**(5).
Priestley, M.J.N. and Park, R. (1987), "Strength and ductility of concrete bridge columns under seismic loading", ACI *Struct. J.*, **84**, 61-76.
Saadeghvaziri, M.A. and Foutch, A. (1990), "Behavior of columns under non-proportionally varying axial load", *J. Struct. Eng.*, **116**(7), 1835-1853.
Sakino, K. and Tomii, M. (1981), "Hysteretic behavior of concrete filled square shell tubular beam-columns failed in flexure", *Transaction of the Japan Concrete Institute (Tokyo)*, **3**, 439-446.
Sakino, K. and Ishibashi, H. (1985), "Experimental studies on concrete filled square steel tubular short columns subjected to cyclic shearing force and constant axial force", *Transactions of the Architectural Institute of Japan* (Tokyo), **353**, 81-89.
Scott, B.D., Park, R. and Priestley, M.J.N. (1982), "Stress-strain behavior of concrete confined by overlapping hoops at low and high strain rates", *ACI Struct. J.*, **79**, 13-27.
Shams, M. and Saadeghvaziri, M. A. (1997), "The state-of-the-art of concrete-filled steel tubular columns", *ACI Struct. J.*, American Concrete Institute, **94**(5).
Shams, M. and Saadeghvaziri, M.A. (1999), "Nonlinear response of CFT columns under axial load", *ACI Struct. J.*, American Concrete Institute, **96**(6).
Sugano, S. and Nagashima, T. (1992), "Seismic behavior of concrete filled tubular steel columns", *Proceedings, Tenth Structural Congress' 92*, ASCE, Apr. 13-15, 914-917.
Taylor, R.L. (1998), "FEAP - A finite element analysis program", University of California.
Wakabayashi, M. and Minami, K. (1981), "Rational analysis of shear in structural concrete columns", *Disaster Prevention Research Institute Annuals*, Kyoto University, **24** B-1 (in Japanese).

Notation

The following symbols are used in this paper:

A_c	: the area of steel section;
A_s	: the area of concrete section;
A_i	: the area of fiber *i*;
$\boldsymbol{B}_1$	: linear part of strain matrix;
$\boldsymbol{B}_n$	: nonlinear part of strain matrix;
$\boldsymbol{B}_u$, $\boldsymbol{B}_w$, $\boldsymbol{B}_\chi$	: strain matrixes correspond to axial, transverse, and curvature displacement;
$\boldsymbol{d}$	: generalized strain matrix;
$\boldsymbol{D}$	: generalized stress matrix;
D	: depth of section;
EA, *EX*, *EI*	: axial, cross-coupling, and flexural stiffness of the section;
E_i^T	: the tangent modulus of concrete or steel for fiber *I*;
f'_{cc}, f'_c	: confined and unconfined compressive strength of the concrete core;
f_y	: yield stress of the steel shell;
$\boldsymbol{K}_t$	: tangent stiffness matrix;
$\boldsymbol{k}_s$	: tangent section stiffness matrix;
L	: element's length;
N	: applied axial force;
N_0	: nominal axial strength $(N_0 = f'_c \cdot A_c + f_y \cdot A_s)$;

$N(x)$, $M(x)$: axial and moment sectional force;
$\boldsymbol{N}_u$, $\boldsymbol{N}_w$: shape functions for axial and transverse deformation;
$\boldsymbol{q}$: nodal displacement vector;
$\boldsymbol{q}_u$, $\boldsymbol{q}_w$: nodal displacement vector correspond to axial and transverse direction;
$\boldsymbol{Q}$: nodal force vector;
$\boldsymbol{Q}_u$, $\boldsymbol{Q}_w$: nodal force vector correspond to axial and transverse direction;
$u(x)$, $w(x)$: axial and transversal displacement of reference axis;
$u'(x)$, $w'(x)$: first derivative of axial and transversal displacement of reference axis respect to local co-ordinate x;
$w''(x)$: second derivative of transversal displacement of reference, axis respect to local co-ordinate x;
V : virtual displacement work;
$\overline{\varepsilon}$: axial strain of axis;
ξ : non-dimensional co-ordinate;
χ : curvature;
Z : descending slope of stress-strain curve of concrete;